A Method for Predicting Dose Distribution of Nasopharyngeal Carcinoma Cases by Multiple Deep Neural Networks

Bilel Daoud*, Ken'ichi Morooka†, Shoko Miyauchi*, Ryo Kurazume*, Wafa Mnejja‡, Leila Farhat‡ and Jamel Daoud‡
*Graduate School of Information Science and Electrical Engineering
Kyushu University, Fukuoka, Japan
†Graduate School of Natural Science and Technology
Okayama University, Okayama, Japan
‡Radiotherapy Department of Habib Bourguiba Hospital
Sfax, Tunisia

***Abstract*—In this paper, we propose a method for predicting dose distribution images of patients with Nasopharyngeal carcinoma (NPC) from contoured computer tomography (CT) images. The proposed system is based on our previous method [1]. The first phase is to obtain the feature maps of 2D dose images of each beam from contoured CT images of a patient by convolutional deep neural network model. In the second phase, dose distribution images are predicted from the obtained feature maps by the integration network. Our modified system predicted dose distribution images accurately. From the experimental results using 80 NPC patients' images, the average number of pixels that satisfy the dose constraints of tumors and OARs regions is 81.9% and 86.1%, respectively. The proposed system had a global 3D gamma passing rates varying from 82.1% to 97.2% for all regions and an overall mean absolute errors (MAEs) was 1.0 $\pm$1.2. From the obtained results, our modified system is superior to the results obtained in our previous system results and conventional methods.**

***Contribution*—The use of the predicted 7-beam weights, as input, into our CNN network leads to improve the predicted dose distribution.**

***Index Terms*—Nasopharyngeal carcinoma, Convolutional neural network, Dose distribution prediction.**

I. Introduction

Nasopharyngeal carcinoma (NPC) is a type of head and neck malignancy occurring in the nasopharynx which lies behind the nose and above the level of the soft palate[2]. One main approach for destroying the NPC cells is an intensity-modulated radiation therapy (IMRT) [3] which is a method for an external beam radiation.

In IMRT, a more focused radiation to the tumor or specific areas within the tumor is delivered while the exposure of healthy tissues is avoided by reducing the radiation dose to the healthy tissues[4]. Therefore, IMRT contributes to the improvement of the Quality-of-Life for NPC patients compared with other radiation therapy techniques and is recommended for over 50% of all cancer to eradicate cancer cells[5].

To eradicate the tumor cells, beams of high energy X-rays (4-20 MV) or electrons (4-25 MeV) from multiple directions are directed through the patient's body to both healthy and cancerous tissues. To minimize the side effects, a prescribed treatment dose of about 70 Gy to the tumor volume is usually delivered with 2 Gy per day for 35 days[6].

Before the prescribed treatment, radiation oncologists plan the IMRT treatment. The planned IMRT treatment is determined by using a treatment planning system. In the planning system, a set of dose objectives of the tumor and organ at risk (OARs), and computed tomography (CT) images are used to determine treatment plan of each beam including its parameters and delivered dose for each target region[7]. However, the current planning systems don't always provide the optimal treatment for a patient. Therefore, the radiation oncologists need to modify the treatment plan repeatedly until the desired dose distribution is approved. Since it takes from several hours to a week to approve the optimal treatment, the modification of the treatment plan is time-consuming. Moreover, the quality of the modification highly depends on the expertise and experiences of the radiation oncologists[8].

Several planning techniques have been developed to determine the optimal IMRT plan [9], [10]. Among them, objective-based planning (OBP)[9] and knowledge-based planning (KBP)[10] are the most famous planning methods. In OBP, a pre-set objectives of dose are used as the input of the planning method to achieve a desirable IMRT. On the contrary, KBP predicts the dose distribution of a new patient from a set of previous plans of irradiated patients. However, these planning methods require suitable handcrafted features, that are complex and tedious to be manually determined, such as spatial information of OARs and tumors, and the number of beams. Therefore, an automatic method for predicting the dose distribution is required to achieve more accurate and effective IMRT treatment.

Recently, deep learning methods using convolutional neural networks (CNNs) have gained great popularity in radiotherapy such as automatic segmentation of organs and tumors[11] and toxicity prediction of radiation therapy plan[12]. Among them,

TABLE I: Detailed information of contoured regions and their labels.

Contours	Dose constraint	Label	Contours	Dose constraint	Label
L/R temporomandibular joint(TMJ)	D_{max} ≤55 Gy	1/2	L/R parotid gland	D_{50} <26 Gy	12/13
Optic chiasma	D_{max} ≤54 Gy	3	Brainstem	D_{1cc} <54 Gy	14
L/R Lens	D_{max} ≤7 Gy	4/5	Spinal cord	D_{1cc} ≤40 Gy	15
Larynx	D_{max} ≤66 Gy	6	PTV(70 Gy)	$D_{95\%}$ ≥66.5 Gy	16
Temporal lobe	$D_{2\%}$ <60 Gy	7	GTV(70 Gy)	$D_{98\%}$ ≥70 Gy	17
L/R Mandible	D_{max} ≤65 Gy	8/9	CTV(70 Gy)	$D_{95\%}$ ≥70 Gy	18
L/R optic nerve	D_{max} ≤55 Gy	10/11			

L/R: Left/Right; D_{max}: maximum dose; D_{50}: 50% of the dose, $D_{2\%}$, $D_{95\%}$, $D_{98\%}$: 2%, 95%, 98% of the dose, respectively; D_{1cc}: 1 cubic centimeter of the dose.

several researches have applied CNN to predict treatment plan[13], [14]. Mahmood et al.[13] employed a new generative adversarial network (GAN) to predict the dose distribution images from 2D contours of tumor and OARs in CT images. Chen et al.[14] predicted the dose distribution by using ResNet 101 whose inputs are tumor and OARs regions. The two methods focused on the direct prediction of dose distribution images from tumors and OARs regions without considering the radiation beam geometry. As mentioned above, the radiation beam geometry influences the quality of the dose distribution.

To solve this problem, in our previous method[1], we proposed a system for predicting the dose distribution images by integrating the predicted dose images of each beam obtained from OARs and tumors regions. The integration process is the sum of predicted dose images obtained by using CNN networks. In this paper, to improve the accuracy of predicting dose distribution, we propose a new method for predicting the dose distribution by incorporating an integration CNN into our previous method.

II. Methods

A. Materials

The data of each patient contains 2D images of the delivered dose, called 2D real dose distribution image, and axial section CT images 256×256[pixels] trimmed from 512×512[pixels] original CT image. From each CT image, two radiation oncologists manually trace all contours of NPC, gross tumor volume (GTV), clinical target volume (CTV) and planning target volume (PTV), and OARs. All pixels in the NPC and OARs regions are assigned a unique teaching label to use as training data for constructing the proposed system. Table I shows the detailed information of NPC and OARs regions, their teaching label, and dose constraints. Here, the dose constraints represent limit delivered doses which are below or above a given threshold for OARs and NPC regions, respectively. In our case, there are five dose constraints: the maximum dose value (D_{max}), 1cubic centimeter (D_{1cc}), and 50% and 95% (D_{50}, $D_{95\%}$) of the dose.

The 2D real dose distribution of NPC patients is constructed from the integration of 2D real dose images of 7 dynamic beams whose orientations are 0, 51, 102, 153, 204, 255, and 306 [deg] around a patient. The spatial resolution of the dose distribution was 0.25×0.25[cm]. Each beam has 6 [MeV] energy and a delivered dose is between 0.27 and 0.34 Gy during 33 days. Therefore, the target dose prescription was 70 Gy in 33 days. By using a set of parameters obtained from a radiotherapy treatment plan, a 2D real dose image of each beam was constructed. An example of the real dose distribution of each beam is shown in Fig. 1. The 2D real dose image of each beam and the 2D real dose distribution are used as a teaching label.

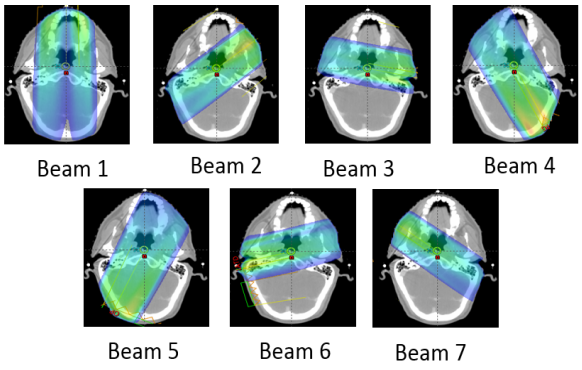

Fig. 1: An example of the dose of each beam.

B. System

Based on our previous system[1] for predicting the dose distribution, the proposed system for predicting the dose distribution consists of two phases. The first phase is to predict the 2D dose image of each beam from its corresponding CT image of a patient. In the second phase, the 2D dose distribution image is estimated by integrating the obtained 2D dose images of all beams. The integration process in our previous system is to sum up all dose values of the 2D dose images of all beams.

On the contrary, the architecture of the proposed system is based on that of of our previous one. The difference to our previous system is to introduce CNN in the integration process. Fig. 2 shows the overview of the new proposed system. The first phase of the proposed method has the same network architecture in[1] to predict the 2D dose images of each beam. Here, the network is an encoder-decoder network which its encoder is composed of two networks with the same architecture. The input of our network is a contoured CT image including the set of the tumors contours, PTV, CTV and GTV, and OARs regions. The output of the decoder is the feature map of the input data of the corresponding beam.

In the second phase of our proposed system, the seven-multiple feature maps obtained from the seven networks are concatenated to multiple feature maps and used as input data for the integration network. The integration network includes 5 convolutional layers and one fully connected layer that

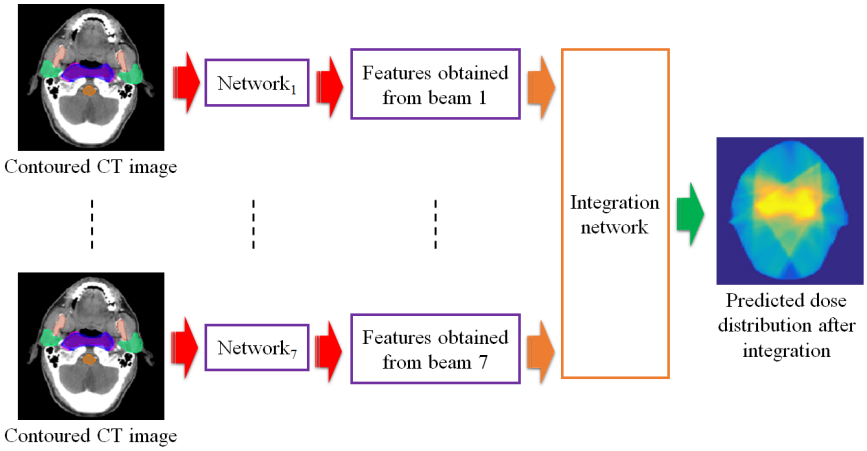

Fig. 2: The architecture of the new proposed method.

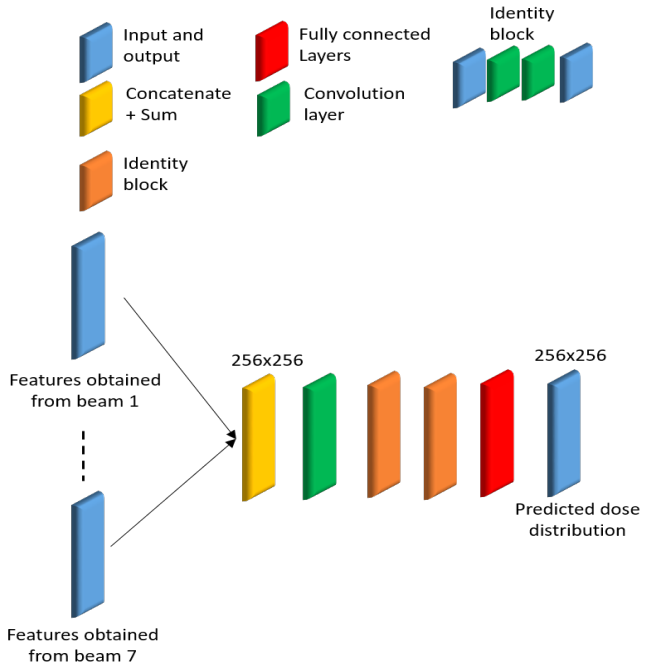

Fig. 3: The architecture of the integration network.

generates the concatenated feature maps to predict the 2D dose distribution images (Fig. 3).

III. Experimental Results

To verify the applicability of our proposed system, we made experiments for predicting the dose distribution using our dataset composed of 80 patient images. The dataset is divided into eight sub-datasets, each of which contains 10 patient images. Therefore, 8-fold cross validation is applied to evaluate the proposed system: 7 sub-datasets are used for training while the rest sub-dataset is employed for testing. The obtained results from our new proposed system are compared with the manual dose distribution by radiation oncologists (MD).

A. Results

In the experiments, the new proposed system is compared with Mahmood et al.[13] (GAN) and Chen et al.[14] (ResNet101) methods. The methods in[13], [14] are downloaded and replaced our network in the first phase to predict dose images of each beam from contoured CT images by using our dataset.

As shown in Fig.4, when the contoured CT image is given as input data (Fig. 4(a)), our network, GAN and ResNet101 with the integration network predict the dose distribution from the image (Fig. 4 (c)-(e), respectively). Fig.4 (b) shows the manual dose distribution image obtained by radiation oncologists and used as the ground-truth.

To compare the proposed system with our previous system in[1], we calculate the number of pixels of each OARs and tumor regions of each patient. Here, the pixels in the OARs and tumor regions are selected so that the dose values of the pixels satisfy the given threshold of the region dose constraint described in Table I. Table II presents the average ratio of the number of pixels to the total number of pixels of OARs and tumors regions of all patients, respectively.

Besides, we compared the accuracy of the proposed network, GAN and ResNet101 by using two 3D gamma analyses. A global 3D gamma analysis with 3%3mm and 4%4mm for $\gamma \leq 1$ was applied to evaluate the obtained results of dose distribution by the three comparison methods. Table III represents the calculated values of the mean pass of 3 D gamma analysis.

Moreover, we evaluated the difference between the predicted OAR and tumor regions of each method with their ground-truth. The evaluation uses the difference between the predicted cumulative dose volume histograms (DVH) of each method and the ground-truth. Here, DVH is the dose value per fractional volume of the target region. A mean absolute error , MAE_{DVH}, of the difference between two DVHs is presented

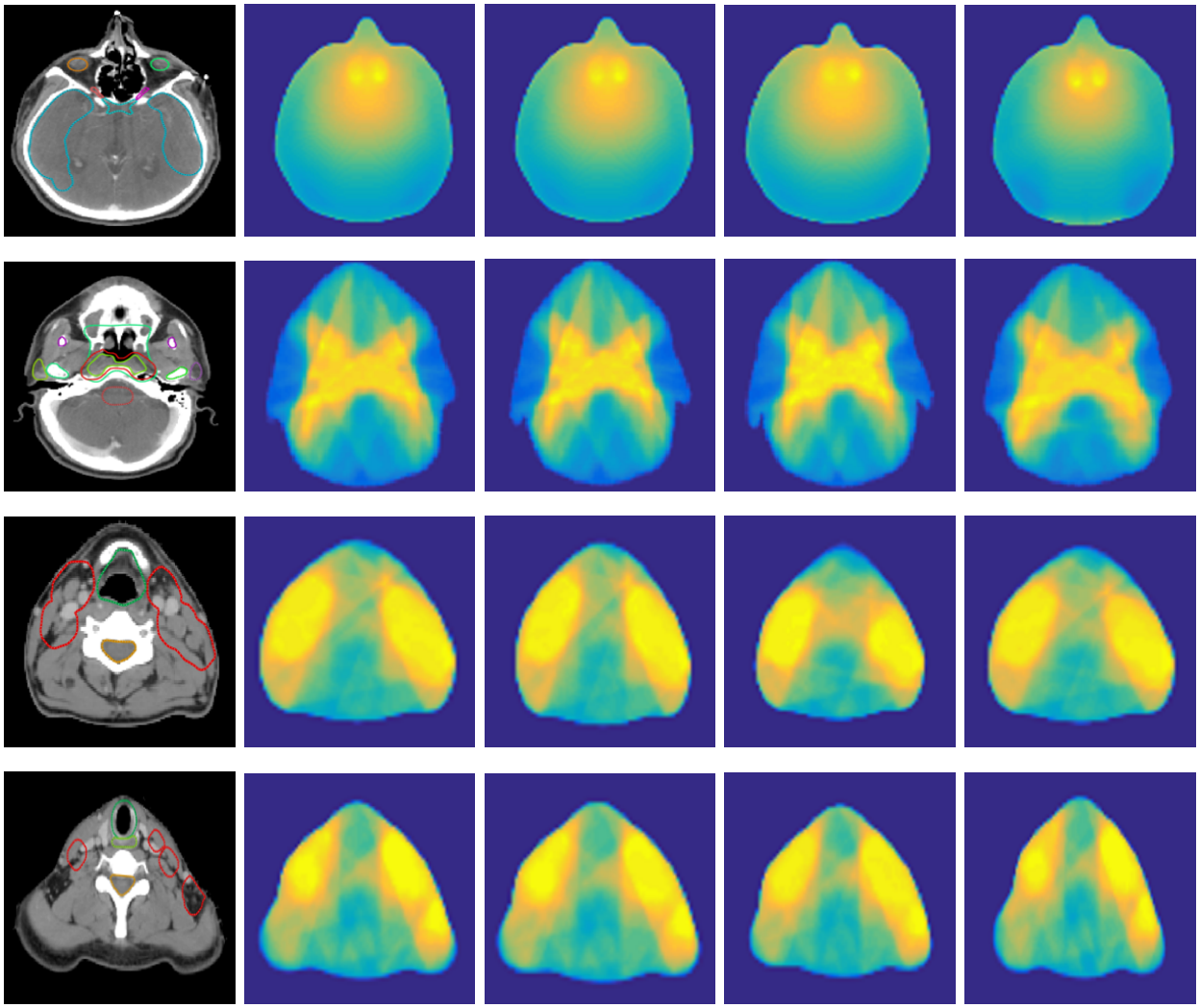

(a) (b) (c) (d) (e)

Fig. 4: Examples of (a)contoured CT image and its dose distribution obtained by (b) Ground-truth, (c)Ours, (d)GAN and (e)ResNet101 with the integration network.

TABLE II: The average number of pixels that its dose values obtained from Ours, GAN, and ResNet101 satisfy the dose constraints of Tumors and OARs regions.

Region	Ours	GAN	ResNet101	Daoud et al.
Tumors	**81.9%**	76.8%	75.6%	76.5%
OARS	**86.1%**	81.2%	82.4%	83.4%

in Table IV. MAE_{DVH} is formulated by:

$$MAE_{DVH} = \frac{1}{m}\sum_{k=1}^{m}\frac{1}{n}\sum_{j=1}^{n}|D_p(j)_{k\%} - D_g(j)_{k\%}|, \quad (1)$$

where *m* is the number of DVH bins separated by 0.01 Gy, *k* is the dose volume index of DVH, *j* is the 2D dose distribution image of the target region, *n* is the total number of images. $D_p(j)_{k\%}$ and $D_g(j)_{k\%}$ are the predicted and the ground-truth doses value at $k\%$ volume of the pixel of the j^{th} image, respectively.

To show the minimum and maximum differences between the predicted region by the three methods and their ground-truth, the DVH of PTV and Larynx of our network, GAN, ResNet101, and their ground-truth are shown in Fig.5 (a) and (b), respectively.

B. Discussion

In the first experiment as shown in Table II, our proposed system with the integration network improves the accuracy of the dose values of the predicted OARs and tumors regions by the three comparison methods: GAN, ResNet101, and our previous system. The integration network leads to the accuracy

TABLE III: Mean pass rates of 3D gamma analysis with 3%3mm and 4%4mm of Ours, GAN, and ResNet101 with the integration network.

	3%/3 mm (%)					4%/4 mm (%)				
	Ours	GAN	p	ResNe101	p	Ours	GAN	p	ResNe101	p
L/R TMJ	**91.8 ± 0.5**	89.5 ± 0.2	0.316	89.9 ± 1.0	0.241	**97.9 ± 0.4**	95.0 ± 0.4	0.233	96.1 ± 1.1	0.188
Optic chiasma	**88.9 ± 0.1**	86.1 ± 1.2	0.213	88.2 ± 1.9	0.112	**97.1 ± 0.1**	95.9 ± 1.1	0.214	96.2 ± 0.5	0.187
L/R Lens	**92.9 ± 3.0**	88.2 ± 0.9	0.401	89.3 ± 1.0	0.319	**98.0 ± 0.6**	95.1 ± 1.2	0.294	95.4 ± 1.7	0.305
Larynx	**82.1 ± 0.4**	77.4 ± 0.6	0.344	77.9 ± 2.3	0.291	**89.4 ± 1.1**	86.7 ± 1.0	0.209	87.5 ± 0.3	0.197
Temporal lobe	**86.9 ± 1.1**	83.8 ± 0.9	0.316	84.4 ± 1.0	0.181	**95.0 ± 0.7**	93.1 ± 1.2	0.183	93.9 ± 0.1	0.167
L/R Mandible	**82.9 ± 0.7**	79.1 ± 1.4	0.288	79.7 ± 0.7	0.240	**93.9 ± 0.6**	88.0 ± 1.9	0.462	87.5 ± 0.6	0.497
L/R optic nerve	**94.5 ± 2.1**	92.3 ± 2.7	0.226	91.9 ± 0.9	0.386	**98.8 ± 1.0**	95.6 ± 2.1	0.274	95.9 ± 0.7	0.228
L/R parotid gland	**89.9 ± 1.4**	87.2 ± 1.1	0.219	87.9 ± 0.4	0.164	**96.0 ± 1.4**	94.7 ± 0.7	0.182	94.6 ± 0.9	0.197
Brainstem	**84.7 ± 1.3**	83.2 ± 0.4	0.113	81.1 ± 0.8	0.247	**92.7 ± 1.8**	91.4 ± 0.7	0.157	89.4 ± 1.2	0.183
Spinal cord	**87.9 ± 2.3**	82.1 ± 1.9	0.397	83.8 ± 0.6	0.344	**95.8 ± 2.7**	92.8 ± 1.4	0.279	93.7 ± 0.9	0.211
PTV	**93.1 ± 4.0**	92.2 ± 1.6	0.112	92.3 ± 0.1	0.149	**99.7 ± 1.3**	98.2 ± 3.7	0.110	98.9 ± 3.2	0.109
GTV	**97.2 ± 2.4**	95.9 ± 0.7	0.219	96.1 ± 1.5	0.154	**98.3 ± 0.1**	96.3 ± 2.7	0.284	96.9 ± 1.3	0.156
CTV	**96.8 ± 2.4**	95.0 ± 1.4	0.187	94.3 ± 0.8	0.233	**99.0 ± 1.2**	98.6 ± 1.3	0.197	98.9 ± 3.5	0.249

TABLE IV: MAE_{DVH} of each region by Ours, GAN, and ResNet101 with the integration network.

Contours	Ours	GAN	ResNet101	Contours	Ours	GAN	ResNet101
L/R TMJ	**0.9 ± 0.9**	1.1± 0.2	1.2± 0.4	L/R parotid gland	**1.2 ± 0.8**	1.7± 0.9	1.6± 1.0
Optic chiasma	**1.2 ± 0.1**	1.7± 0.6	1.3± 0.7	Brainstem	**1.1 ± 0.9**	1.2± 0.4	1.6± 0.1
L/R Lens	**1.3 ± 0.8**	1.7± 1.2	1.6± 0.3	Spinal cord	**1.3 ± 0.4**	1.4± 0.7	1.4± 0.6
Larynx	**1.5 ± 0.4**	2.3± 0.8	1.8± 0.7	PTV	**0.8 ± 0.4**	1.0± 0.6	1.1± 1.7
Temporal lobe	**0.9 ± 0.7**	1.5± 0.3	1.2± 1.1	GTV	**0.8 ± 0.6**	1.1± 0.1	0.9± 1.6
L/R Mandible	**1.0 ± 0.7**	1.2± 0.9	1.3± 0.7	CTV	**0.7 ± 0.1**	1.1± 0.7	0.9± 0.5
L/R optic nerve	**0.8 ± 1.6**	1.3± 0.3	1.2± 0.6				

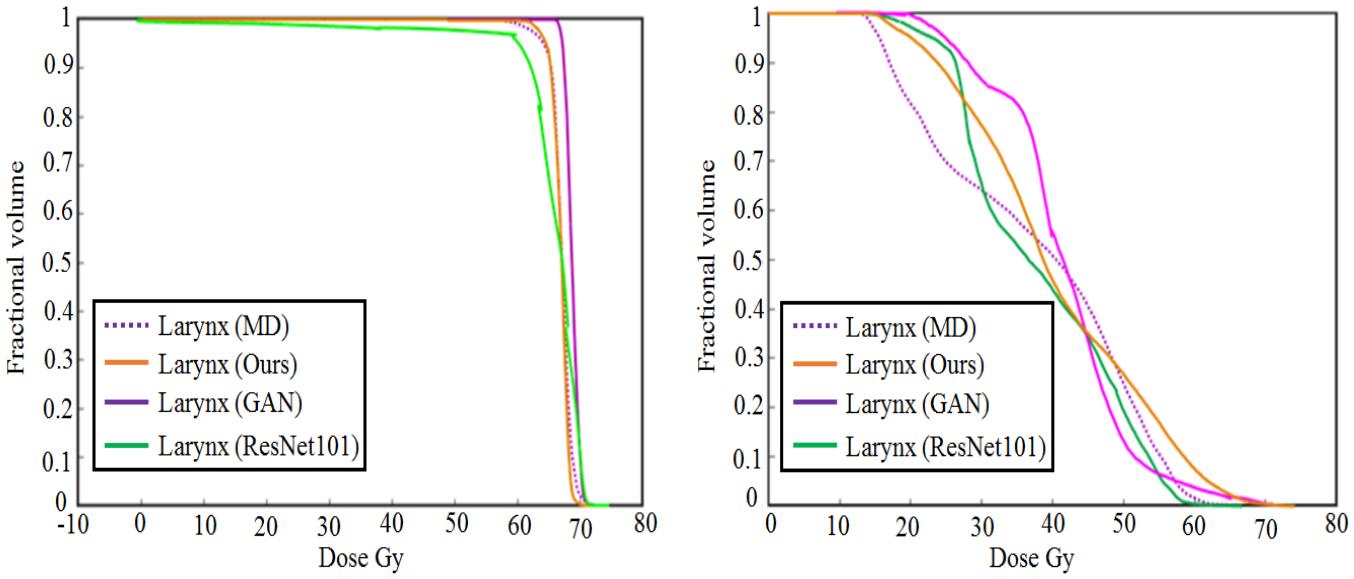

(a) DVH of PTV

(b) DVH of Larynx

Fig. 5: DVH of three methods with the integration network vs the ground-truth.

improvement of estimating a dose distribution image including OARs and tumors regions.

From Table III, the mean pass rates of 3D gamma of our network is higher than those of GAN and ResNet101 for all OARs and tumors regions. Moreover, from Table IV, MAE for most OARs and tumors using the proposed method is the smallest among the two methods. From the global 3D gamma analysis with 3%3mm and 4%4mm for $\gamma \leq 1$, the mean pass rates of all regions with our network is higher than those with GAN and ResNet101 methods. To compare our network, GAN, and ResNet101, statistical analysis is performed with paired t-tests (p-value <0.05). From the paired t-test, there are no significant difference between our network and the two comparison methods for all regions.

Owing to these, our network with the integration network can predict almost the same dose distribution as the ground-truth compared with GAN and ResNet101. In addition, our network with the integration network results in the high accuracy of predicting small volumes of OARs such as Left and right Lens because of the following reason. By training OARs and tumors regions separately in our network, the network trains the dataset with more detailed information and outputs better features maps compared to the two comparison methods. In addition, using useful feature maps, the integration network can estimate reliable dose distribution images.

IV. Conclusion

In this paper, we present a method for predicting the dose distribution for a patient from contoured CT images. Extending our previous method[1], the proposed method introduces an integration CNN that predicts the dose distribution from the obtained feature maps of seven beams. The experimental results show that our proposed system improves the accuracy of predicting dose distribution compared with conventional methods.

In this work, we focused on the prediction of the dose distribution from the obtained feature maps of seven beams without considering dose constraints of OARs and tumor regions and the relation between the two phases. One of our future works is to train the integration network with an optimization function that contains dose constraints of all contours to improve the prediction accuracy of dose values in the predicted dose distribution.

Acknowledgment

This work was supported by JST CREST Grant Number JPMJCR20F3, Japan.

References

[1] D. Bilel, M. Ken'ichi, M. Shoko, K. Ryo, M. Wafa, F. Leila, and D. Jamel, "Dose distribution prediction for optimal treamtment of modern external beam radiation therapy for nasopharyngeal carcinoma," in *Workshop on Artificial Intelligence in Radiation Therapy*. Springer, 2019, pp. 128–136.

[2] M. L. Chua, J. T. Wee, E. P. Hui, and A. T. Chan, "Nasopharyngeal carcinoma," *The Lancet*, vol. 387, no. 10022, pp. 1012–1024, 2016.

[3] K. Au, R. K. Ngan, A. W. Ng, D. M. Poon, W. Ng, K. Yuen, V. H. Lee, S. Y. Tung, A. T. Chan, H. C. Sze *et al.*, "Treatment outcomes of nasopharyngeal carcinoma in modern era after intensity modulated radiotherapy (imrt) in hong kong: a report of 3328 patients (hknpcsg 1301 study)," *Oral oncology*, vol. 77, pp. 16–21, 2018.

[4] W. XiaoShen and E. Avraham, "Imrt for head and neck cancer: reducing xerostomia and dysphagia," *Journal of radiation research*, vol. 57, no. S1, pp. i69–i75, 2016.

[5] A. Edvard, S. Ewa, and N. e. a. Jan, "Impact on quality of life of imrt versus 3-d conformal radiation therapy in head and neck cancer patients: A case control study," *Advances in radiation oncology*, vol. 2, no. 3, pp. 346–353, 2017.

[6] E. M, Y. MA, B. F, and M. MR, "A planning study to optimise a simultaneously integrated boost treatment of larynx cancer with seven intensity-modulated radiation therapy (imrt) beams," *Journal of Radiotherapy in Practice*, vol. 17, no. 4, pp. 447–454, 2018.

[7] P. Scott, Z. Rafał, C. Margherita, B. Mark, C. Yair, and S. Reinhard, "Sparsity constrained split feasibility for dose-volume constraints in inverse planning of intensity-modulated photon or proton therapy," *Physics in Medicine & Biology*, vol. 62, no. 9, p. 3599, 2017.

[8] B. Isabel J, P. Anthony J, X. Beibei, and e. a. Ezra EW, Cohen, "Importance of radiation oncologist experience among patients with head-and-neck cancer treated with intensity-modulated radiation therapy," *Journal of Clinical Oncology*, vol. 34, no. 7, p. 684, 2016.

[9] X. Ilma, W. Eugene, B. Karl, L. Michael, and C. Jeff Z, "Automated imrt planning with regional optimization using planning scripts," *Journal of applied clinical medical physics*, vol. 14, no. 1, pp. 176–191, 2013.

[10] L. Nan, C. Ruben, and e. a. Igor, Sirak, "Highly efficient training, refinement, and validation of a knowledge-based planning quality-control system for radiation therapy clinical trials," *International Journal of Radiation Oncology* Biology* Physics*, vol. 97, no. 1, pp. 164–172, 2017.

[11] D. Bilel, M. Ken'ichi, K. Ryo, M. Wafa, F. Leila, and D. Jamel, "3d segmentation of nasopharyngeal carcinoma from ct images using cascade deep learning," *Computerized Medical Imaging and Graphics*, vol. 77, p. 101644, 2019.

[12] I. Bulat, T. Diego AS, C. Daniel T, Y. Yixuan, K. Albert C, and X. Lei, "Automated hepatobiliary toxicity prediction after liver stereotactic body radiation therapy with deep learning-based portal vein segmentation," *Neurocomputing*, vol. 392, pp. 181–188, 2020.

[13] M. Rafid, B. Aaron, M. Andrea, D. Adam, and C. Timothy CY, "Automated treatment planning in radiation therapy using generative adversarial networks," *arXiv preprint arXiv:1807.06489*, 2018.

[14] C. Xinyuan, M. Kuo, L. Yexiong, Y. Junlin, and D. Jianrong, "A feasibility study on an automated method to generate patient-specific dose distributions for radiotherapy using deep learning," *Medical physics*, vol. 46, no. 1, pp. 56–64, 2019.